Master's Thesis

Emittance measurement system for MAX IV PC RF gun

Marcus Isinger

Department of Electrical and Information Technology,
Faculty of Engineering, LTH, Lund University, January 2015.
In cooperation with MAX IV Laboratory.

Emittance measurement system for MAX IV PC RF gun

LUND
UNIVERSITY

Marcus Isinger
Department of Electroscience
Lund University

A thesis submitted for the degree of
Master of engineering physics

2014 December

Abstract

In this thesis I present the development of an emittance measurement device for the MAX IV photocathode RF gun and the implementation of a method for analyzing and estimating the beam emittance from the data. The emittance of an electron beam is important for the amplification process in a Free Electron Laser (FEL). The smaller the emittance is, the more efficient is the light amplification. This is of interest for the Free Electron Laser that is planned for MAX IV in Lund. To reach a small emittance, a technique called emittance compensation will be used.

To measure the emittance the research group working on the MAX IV FEL decided to use an emittance meter. This device was built at SPARC in Italy and is placed at MAX IV in Lund. The device was equipped with new motors and cameras where needed. The photocathode RF gun was installed in the available test stand and all auxiliary parts were connected.

Multiple simulations were run to evaluate not only the effect of the parameters of the laser beam on the electron beam emittance, but also the performance of the emittance estimation method.

It was not possible to test the emittance meter in time, but old data showed that a single slit method produces a signal better suited for the emittance estimation method than a one shot pepperpot method does.

Acknowledgements

I am using this opportunity to express my gratitude to everyone who supported me throughout the course of this thesis. I am thankful for their guidance, constructive criticism and friendy advice during the project work.

I express my warm thanks to my supervisors Dr. Francesca Curbis and Joel Andersson for their support and guidance.

Furthermore I would also like to acknowledge with much appreciation the crucial role of the staff of MAX IV, who not only gave the permission to use all required equipment and material, but also lent me a hand when needed.

Thank you,

Marcus Isinger

Contents

List of Figures

List of Tables

1

Introduction

1.1 MAX IV

MAX IV is a new synchrotron radiation facility being built in Lund, Sweden, that primarily generates light in the X-ray region. The linear accelerator that feeds the two storage rings has been designed for a possible expansion to a Free Electron Laser (FEL). A conceptual design study is foreseen and the target is to have an FEL at the MAX IV linac within 10 years [4]. The proposed layout is seen in figure 1.1, where much of the existing accelerator structure is used.

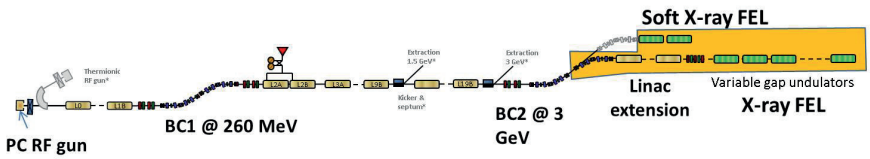

Figure 1.1: MAX IV FEL layout - Layout of the planned FEL at MAX IV, where the extension to the existing linac is highlighted [5].

1.2 Introduction to a Free electron laser

An X-ray laser source would have many characteristics that the majority of X-ray techniques could benefit from. Some of these are high intensity and brightness, collimation, spatial coherence and monochromaticity. Conventional lasers are limited to much longer wavelengths and until very recently, no laser was available for X-ray wavelengths. In 2009 the LCLS at Stanford

achieved its first lasing, paving the way for new FEL facilities around the world [1]. Since then a few facilities are being built that are expected to be operational in the years to come.

A Free Electron Laser is fundamentally different from a conventional laser. Where a laser uses optical pumping to create a population inversion of states in a gain medium, an FEL uses accelerated free electrons, free in the sense that they are not bound to an atom [2]. Instead of using a cavity to induce stimulated emission, most FELs use the interaction between the electron beam and the electromagnetic field to achieve the same effect. Direct exchange of energy between the electrons and the laser beam is not possible without a horizontal velocity component of the beam. This is introduced by letting the beam through an undulator, creating a horizontal component which the electric field of the FEL beam can couple to. The energy transfer can go both ways, depending on the phase between the electron trajectory and the laser field. For a positive energy yield an electron needs to cross the midpoint of its oscillation as the electric field, traveling alongside, reaches its maximum, resulting in a deceleration of the electron and an energy transfer to the field. Since the field travels slightly faster than the electrons, the phase shift of the field needs to be $\Delta\Phi = \pi$ for the field to change sign when the electron crosses the midpoint again.

The wavelength of the radiation emitted in the forward direction in the FEL is given by

$$\lambda_m = \frac{1}{m} \cdot \frac{\lambda_u}{2\gamma^2} \left(1 + \frac{K^2}{2}\right) \quad m = 1, 3, 5... \tag{1.1}$$

where m is the harmonic number and K is the dimensionless undulator parameter

$$K = \frac{eB_0\lambda_u}{2\pi m_e c} \tag{1.2}$$

Equation (1.1) is the same expression for spontaneous emission in an undulator, where the undulator period is denoted λ_u while γ is the ordinary relativistic factor, e is the elementary charge, B_0 is the magnetic field strength, m_e is the electron mass and c is the speed of light in vacuum. The wavelength can thereby be controlled by varying the undulator gap. For a complete derivation, see [2] chapter 9.

The spontaneous emission can be amplified by the FEL process briefly described above if the electron beam quality is sufficiently high. This process is called Self Amplified Spontaneous Emission (SASE). For efficient beam-radiation interaction, the transverse emittance should fulfill the diffraction limit condition

$$\varepsilon \leq \frac{\lambda}{4\pi} \tag{1.3}$$

where λ is the wavelength of the emitted radiation [3]. The FEL beam will be subject to diffraction, and the resulting widening could spoil the good overlap with the electron beam and reduce the energy transfer from the electrons to the light. The condition above is a very demanding condition and can often not be fully satisfied.

1.3 Emittance compensation

As shown in the previous section, one crucial component in the process of operating an FEL is achieving an extremely low emittance electron beam. A low emittance aids the lasing process and results in a higher brilliance light beam. The emittance easily grows as the beam travels through the accelerator due to the inherent space charge forces of the beam [3]. This force originates from the negative charges of the electrons and becomes stronger the more dense the bunch is. There is fortunately a way to counteract this effect by using a scheme called *emittance compensation*. The scheme prescribes that one wants a focused beam at the entry of the linear accelerator. Due to the emittance oscillations that the beam undergoes as it is extracted from the cathode, one wants to find a setting where the emittance evolution shows a local maximum just before the linac entry. It is then possible to lock the emittance at very low values as the beam exits the linac. This working point should be about 1.5 m away from the cathode at the MAX IV FEL, since this is where the linac begins. The setup is configurable to some degree.

1.4 Aims of the project

The main goal is to measure the emittance evolution of the electron beam generated by the photocathode RF electron gun at MAX IV. The emittance evolution is compared with simulated results of the RF-gun. The emittance along the z-axis must show a double minimum behavior at the linac entry as mentioned earlier.

There will be several preliminary tasks to be accomplished on the way, one of those is to build an automatic emittance measurement system for measuring the emittance of the beam. Another is to write a MATLAB script simulating a measurement to evaluate the measurement method.

2

Theory

2.1 Emittance

Emittance is a property of a particle beam that characterizes its size and divergence. If we define two phase space variables for each spatial variable, namely the position and momentum components of the particle, the emittance is a volume in this phase space. These coordinates are often taken to be the offsets from those of an ideal particle. Unlike the physical parameters of the beam, the emittance is invariant in the absence of dissipative forces and is as such a convenient parameter for describing a particle beam.

If we have a beam of of N identical particles with no mutual interaction, only the canonical phase space can be considered. This is a 6-dimensional space in which the distribution function $f(x, y, z, p_x, p_y, p_z, t)$ is described. The N particles form a beam only if they are clustered in a small region and if N is large they can be represented by a phase density such that at time t the number dN of particles in a small volume d^3qd^3p of phase space is given by

$$dN = f(\vec{q}, \vec{p}, t)d^3qd^3p \tag{2.1}$$

The phase density $f(\vec{q}, \vec{p}, t)$ can be viewed as a probability distribution in the phase space and commonly it is represented as a Gaussian distribution. Often the complete phase space can be split into a transverse and longitudinal space if the two are decoupled. Should the transverse motions be independent of one another as well, the phase space can be reduced to two 2-dimensional spaces x, p_x and y, p_y [6]. A typical phase space plot consists of a point for each particle's phase space coordinate for a specific time.

If the transverse momentum components are negligible compared to the longitudinal, i.e. $p_z >> p_x, p_y$, then x' and y' can be taken to be the transverse angles with respect to the ideal trajectory [7]. The new coordinate space with (x, x', y, y') is called trace space to distinguish it from phase space.

The emittance can now be defined in two different ways, either with an analytical or with a statistical approach. Here we will look into the statistical approach, for the analytical one see [7] and [2] where it is evident that the emittance is the area of an ellipse in a 2-dimensional phase space. The statistical definition of emittance is based purely on the distribution of particles in trace space. This approach is more practical for particle simulations and measurements.

Let the coordinates of a 2D trace space be position w and angle w'. The second-order moments of a distribution of N points on the $w - w'$-plane, with the origin chosen so that the average position and angle of the points are zero, are then given by

$$\sigma_w = \sqrt{\frac{1}{N}\sum_{i=1}^{N} w_i^2} \qquad \sigma_{w'} = \sqrt{\frac{1}{N}\sum_{i=1}^{N} (w_i')^2} \tag{2.2}$$

If we orient the axis so that σ_w is maximized while $\sigma_{w'}$ is minimized we may define the area, or emittance, of the $w - w'$ distribution as the witdh in w multiplied by the width in w'

$$\varepsilon = 2\sigma_w 2\sigma_{w'} = 4\sqrt{\sigma_w^2 \sigma_{w'}^2} \tag{2.3}$$

The reference coordinate axes of a measured, or simulated, distribution may be rotated or translated so that the above expression is not valid. In [7] it is shown that the emittance can be expressed in the actual coordinates x and x'. The resulting expression in equation (2.4) is written only in terms of $< x^2 >$, $< (x')^2 >$ and $< xx' >$.

$$\varepsilon_x = \sqrt{< x^2 >< (x')^2 > - < xx' >^2} \tag{2.4}$$

When a beam is accelerated, the longitudinal momentum component increases while the transverse component is unchanged, resulting in a smaller transverse angle. To compensate for this, a normalized emittance ε_N is introduced, which is scaled according to the beam energy, $\varepsilon_N = \beta\gamma\varepsilon$ and is thereby invariant.

2.2 Ferrario working point

Two different kinds of emittance, slice and projected, have to be considered when analyzing the efficiency of the FEL process. Figure 2.1 illustrates how a gaussian distributed bunch is divided into slices in phase space. The total projection of the slices is obtained as the weighted sum of the slice phase space contributions [8], as figure 2.2 shows. These slices can move relative one another in phase space, giving rise to oscillations in the projected emittance. There are no methods available at MAX IV that can measure the slice emittance of a bunch.

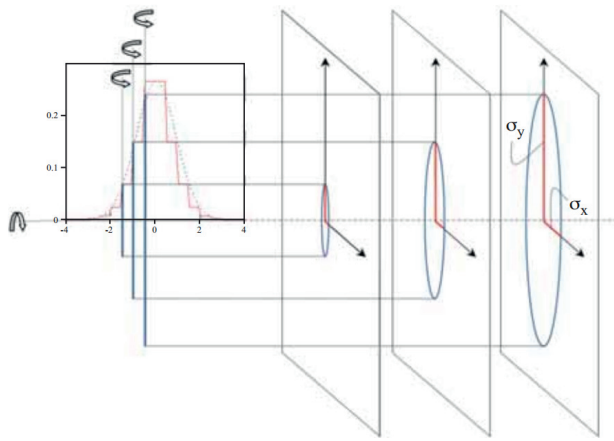

Figure 2.1: Slice phase space - Illustration of how a gaussian distributed bunch is divided into slices in phase space [8].

Furthermore, when electrons are extracted from an RF photocathode the emittance evolution of the beam undergoes cold plasma oscillations. In a study by M. Ferrario et al. for Stanford Linear Accelerator Center, motivated by a redesign of a photoinjector for their free electron laser (LCLS), they discovered a new effective working point for a split RF photoinjector [9]. If they increased the strength of the solenoid field in the gun, the emittance evolution showed a double minimum behavior in the drifting region, as seen in figure 2.3. By placing the linac where the local emittance maximum and the beam waist envelope occurs, the second emittance minimum can be shifted to the booster exit and frozen at a very low level.

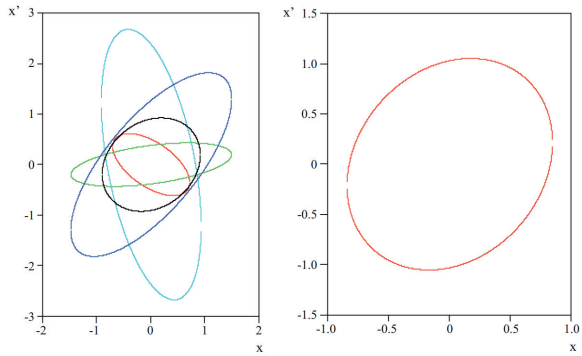

Figure 2.2: Slice and projected phase space - Illustration of slices in phase space and their projection [8].

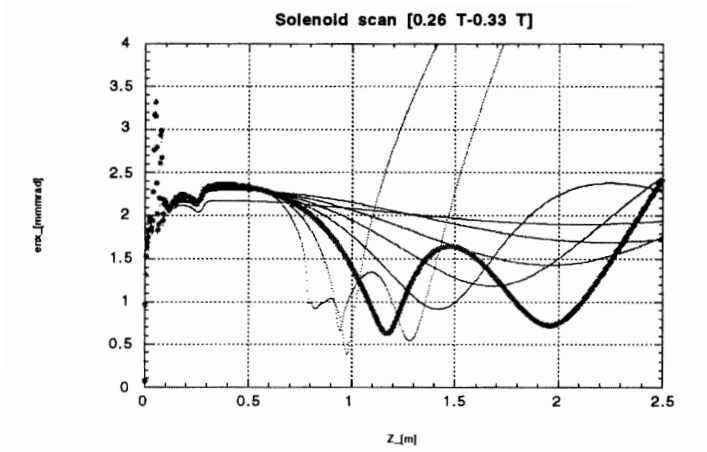

Figure 2.3: Emittance - Emittance evolution for different solenoid strengths. The double minimum behavior is highlighted [9].

2.3 Emittance measurement

A simple yet effective way of measuring the emittance of a beam is with a slit. A plate with multiple slits, henceforth called a multi-slit, is seen in figure 2.4. It works by dividing an incident space-charge dominated beam into smaller beamlets, each with a very low charge in order to reduce the influence it has on the divergence. Figure 2.5 shows a typical setup of an emittance measurement. Two coordinates are used to locate the beamlets, x for the slit and X for the screen, while L is the distance between the two. The origins of the coordinate systems need not be aligned, but are assumed to have the same unit. The slits are assumed to be small compared to the beam size and there is no overlap between the spots on the screen. The goal is to express equation (2.4) in terms of the geometrical parameters of the holes and the beamlet spots.

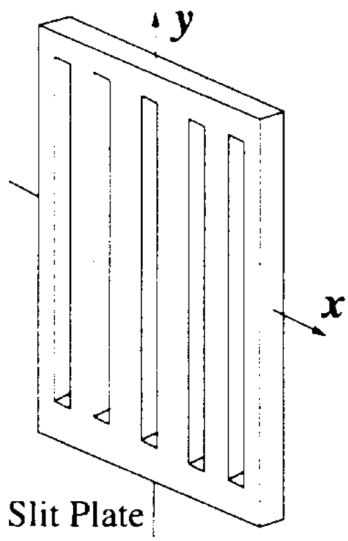

Figure 2.4: Multi-slit plate - Schematic of a multi-slit plate [10].

The method decribed here for calculating the emittance is the one Zhang developed in [10]. It was developed for a slit but is easily generalized to a pepperpot, a two-dimensional version of a slit.

Assume a total number of M particles before the slit and N particles after with positions

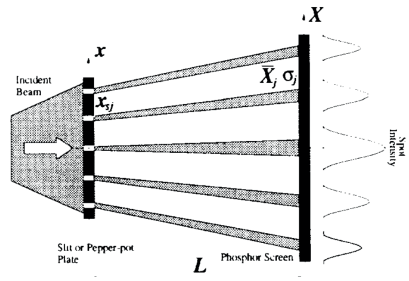

Figure 2.5: Setup - Cross section of a typical setup. The incident beam comes from the left and hits the phosphor screen on the right [10].

(x_i, y_i) and momenta (x'_i, y'_i). The rms emittance is then found to be

$$\begin{aligned} \varepsilon_x^2 &\equiv < x^2 >< (x')^2 > - < xx' >^2 \qquad (2.5) \\ &\approx \frac{1}{N^2}\left(\left[\sum_{j=1}^{p} n_j(x_{sj} - \bar{x})^2\right]\left[\sum_{j=1}^{p}(n_j\sigma_{x'_j}^2 + n_j(\bar{x'_j} - \bar{x'})^2)\right] - \left[\sum_{j=1}^{p} n_j x_{sj}\bar{x'_j} - N\bar{x}\bar{x'}\right]^2\right) \end{aligned}$$

Here, x_{sj} is the j:th slit position, p is the total number of slits and n_j is the number of particles through the j:th slit. n_j is practically a weighting of spot intensity. $\bar{x}$ is the mean position of all beamlets, calculated using the slit positions as in equation (2.6).

$$\bar{x} = \frac{1}{N}\sum_{j=1}^{p} n_j x_{sj} \qquad (2.6)$$

The mean divergence of the j:th beamlet $\bar{x'_j}$ is obtained from equation (2.7) where $\bar{X}_j$ is the mean position of the j:th spot on the screen.

$$\bar{x'_j} = \frac{\bar{X}_j - x_{sj}}{L} \qquad (2.7)$$

Then the mean divergence of all beamlets is simply

$$\bar{x'} = \frac{1}{N}\sum_{j=1}^{p} n_j \bar{x'_j} \qquad (2.8)$$

Finally, the rms divergence of the j:th beamlet is defined as

$$\sigma_{x'_j} \equiv \frac{1}{L}\sqrt{\frac{1}{n_j}\sum_{i=1}^{n_j}(X_{ji} - \bar{X}_j)^2} \tag{2.9}$$

where X_{ji} is the spot position for the j:th slit. As seen, the emittance is now expressed solely in terms of measurable parameters. The above formulas are of course valid for y as well. To generalize these for a pepperpot, seen in figure 2.6, you only need to sum all spots in y for ε_x and vice versa for ε_y.

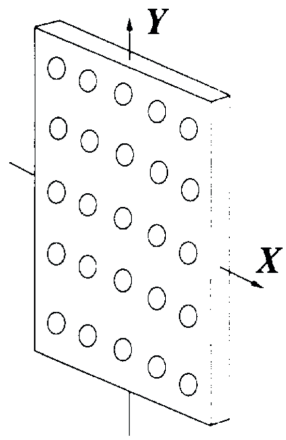

Figure 2.6: Pepperpot plate - Schematic of a pepperpot plate [10].

2.4 Slit dimensions

The dimensions of the slit plate are vital for the method to work as expected. First of all, the slit width needs to be small compared to the beam, otherwise the approximation made in the emittance formula will not hold. Secondly, not all electrons hitting the slit plate beside a slit will be stopped by the plate, contributing to the background noise. To reduce the noise a thicker slit plate would be desirable, but in reality angular acceptance and manufacturing considerations call for a thin plate. The noise is also reduced by electron scattering in the plate, that can even be the dominating factor of noise removal. In [11] they found that with a pepperpot made out of a copper plate, a signal to background ratio of above 100 is reached with a thickness of 1.5 mm for an energy of 20 MeV. The CSDA[1] range of an electron at this energy is 1.1 cm [12]. Copper was chosen because of its high heat conductivity to quickly disperse the deposited energy. Finally, the spacing of the slits determines the number of beamlets and the spacing between them. The spacing needs to be large enough so that the spots on the screen do not overlap, while still maintaining a sufficiently large spot size for a precise reading by the CCD camera. In [11], they also investigate the spacing's effect on the phase space representation with a pepperpot. The results show that it is possible to achieve an accuracy of 10% within the real emittance as long as the hole distance of the pepperpot is equal to or less than the rms beam size.

[1] The *Continuous Slowing Down Aproximation* is a very accurate approximation of the average range of a charged particle in matter. It is obtained by integrating the total stopping power of the material with respect to the energy.

3

Method

3.1 Experimental setup

The device used to measure the emittance is shown in figure 3.1. This emittance meter was built at SPARC, Italy, and allows for measuring the emittance at varying distances from the cathode [13]. It consists of two long bellows and two paddles with a short bellow in between them, making it possible to measure the rms emittance at distances in the range 170 cm to 370 cm. The first paddle comprises a slit and the second a scintillator screen, and these two can move relative each other. The radiation from the YAG screen is emitted in the forward direction, to the right in the figure, and collected by a 45 degree screen at the second paddle. Beam images are then acquired with a CCD camera pointing at the screen equipped with a macro lens, resulting in a resolution of 15.4 µm per pixel. All movable parts are driven by stepper motors. Before the start of this thesis project, the emittance meter had not been operating for many years, therefore all motors were replaced and their controls were substituted with a system called TANGO [14]. TANGO is an overhead toolkit system that supports binding to MATLAB which means the emittance device can be run almost entirely from MATLAB.

To generate electrons, the setup uses a photocathode electron gun, shown in figure 3.2. Radio-frequency fields are supplied through the top via a waveguide, creating an electric field inside the gun cavity. A laser pulse is directed through the opening where the beam leaves, hitting the copper plate marked “cathode” in the image. If the pulse has enough energy to extract electrons, the field inside the gun accelerates these electrons in the direction illustrated in the zoomed image.

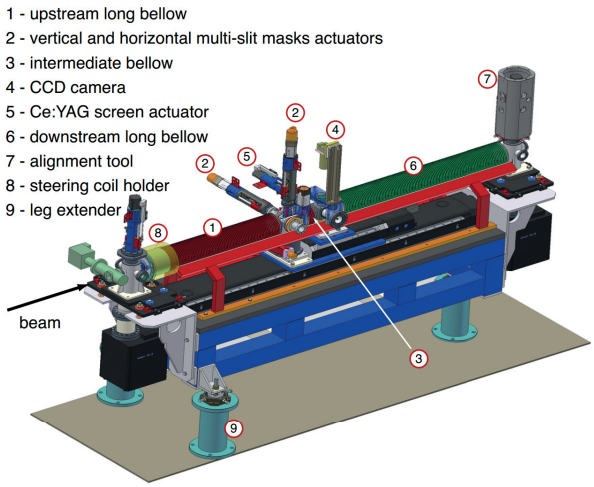

Figure 3.1: Emittance meter - Schematic of the emittance meter, developed at SPARC [13].

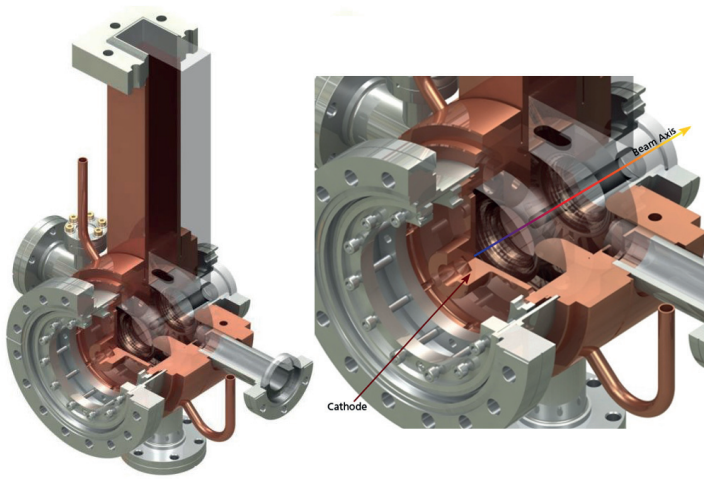

Figure 3.2: Electron gun - Schematic of the photo-cathode electron gun that is used in the setup [15, 16].

The final setup is shown in figure 3.3, where the entrance to the emittance meter is visible behind the yellow fluorescent paper on the laser table. In the left side of the picture the copper electron gun is shown, bolted to an alignment plate allowing for small adjustments. It has three ion pumps connected to it and a waveguide vertically directed to a klystron. Just to the right of the gun sits a solenoid, the blue cylinder in the picture, with the purpose of focusing the electrons. The electrons then travel through a valve, a current transformer[1] and the laser chamber before arriving at the emittance meter. The laser chamber has a small window through which the laser beam is transmitted. The laser beam emerges from the ceiling down onto the laser table, where it is pointing at a movable mirror outside the chamber window. From there it is reflected to hit the cathode of the electron gun.

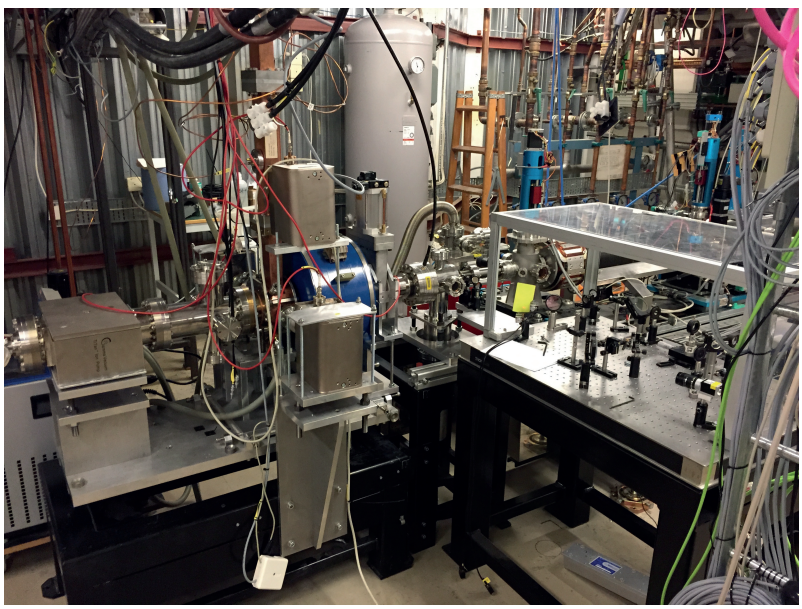

Figure 3.3: Final setup - Image of the final setup with the electron gun connected to the emittance meter.

[1] A current transformer is a device capable of measuring a beam current non-destructively.

3.2 Simulations

Two different simulations are carried out to assess the behavior of the emittance evolution of the beam, as it travels through the setup, and the performance of the estimation procedure.

The simulations are mainly carried out in Astra while additional calculations and manipulations are done in MATLAB. Astra (A Space Charge Tracking Algorithm) [17] is a program developed at DESY and is available on Windows and Linux. It tracks particles through user defined fields taking into account the space charge field of the particle cloud. The tracking is based on a non-adaptive Runge-Kutta integration of fourth order. All simulations were run on an "Ivy Bridge" 2.3 GHz Intel Core i7 processor. Only one processor core was utilized by Astra and MATLAB.

The first simulation shows how the emittance evolution is affected by changes in different parameters and then attempt to find the double minimum behavior of the emittance evolution for the MAX IV RF gun. The second simulates a pepperpot measurement to evaluate the performance of the method in two dimensions.

3.2.1 Emittance evolution

There is a wide range of parameters that affect the outcome of the emittance evolution. Not only the magnitude of the solenoid field and electric fields in the RF gun, but also the shape of the laser pulse that hits the cathode. Multiple simulations were run while varying all parameters individually to see how they each affect the emittance. In all simulations 1000 electrons were used. This number is a bit too low to get an accurate result in some cases, but a simulation shows that it generates sufficiently accurate results for the purpose of this study. Increasing the number of particles to 10000 increases the computation time by roughly a factor of four. The energy of the impinging photons from the laser was set to 4.71 eV, corresponding to a wavelength of 263 nm, and the effective work function of the cathode to 4.26 eV. The shape of the electric field applied over the cathode is shown in figure 3.4 and the shape of the magnetic field from the solenoid in figure 3.5. These fields were fed to Astra, which scales them according to a maximum value. The particles were tracked from the cathode, at $z = 0$ m, to a distance of 3 m away ($z = 3$ m).

The frequency of the electric field was set to 2.998 545 GHz, leaving the following parameters to vary: the maximum electric field, the maximum magnetic field, the phase shift between the electric field and the triggering of the laser, the shape of the laser pulse which in turn affects

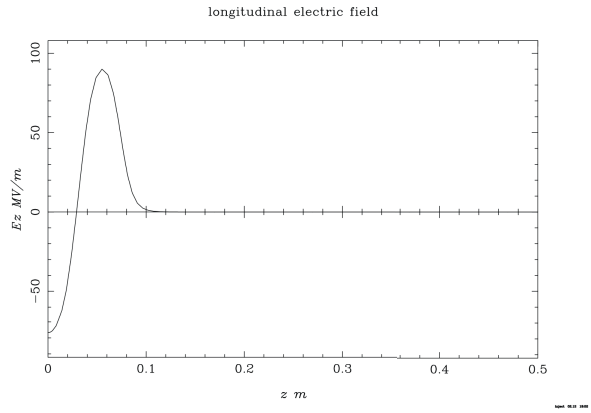

Figure 3.4: Electric field - The shape of the electric field applied over the cathode. The magnitude of the field can be scaled by Astra.

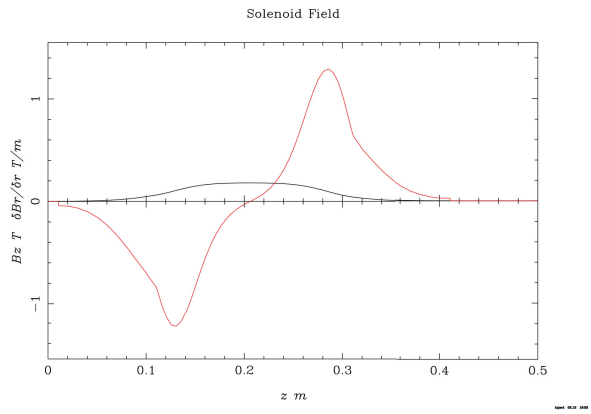

Figure 3.5: Magnetic field - The shape of the magnetic field from the solenoid along with its derivative. The magnitude of the field can be scaled by Astra.

the charge and size of the electron bunch. MATLAB was set up to loop trough a variety of combinations and then plot the emittance and beam envelope calculated by Astra.

3.2.2 Pepperpot simulation

To simulate the pepperpot measurement, a lot more particles are needed since most of them will not make it through the pepperpot. This will of course affect the computation time negatively. A number of 100 000 particles was chosen, which lets enough particles through while keeping the computational time manageable. The simulation was then carried out in four steps. First, the same distribution as above was generated, although with more electrons, and Astra tracked this particle cloud from $z = 0\,\mathrm{m}$ to about $z = 1.5\,\mathrm{m}$, depending on where the pepperpot was placed. The particle files generated by Astra were then imported to MATLAB which iterated through each electron, removing those whose position did not align with the grid of the hypothetical pepperpot. The dimensions of the pepperpot were varied based on the width of the beam envelope. The stripped particle distribution was then fed to Astra again, tracking the electrons from the pepperpot to a fictitious screen 0.1 m - 0.4 m away from the pepperpot. There they were imported to MATLAB for emittance analysis.

The emittance was calculated the same way it would be using real measurements. That is, the particle distribution at the screen was plotted and the image was then summed horizontally and vertically. This generates two one-dimensional plots, consisting of a number of peaks representing the dots on the screen. The peaks were identified using an external script called *findpeaksfit*, which is part of a peak finding package for MATLAB [18]. The script indentifies a peak by looking for downward zero-crossings in the first derivative that exceeds a certain threshold. It then fits a curve, in this case a gaussian, to each peak and calculates the residual. The width, position and area of the gaussian peaks were then used to evaluate equations (2.6) to (2.9), which were then inserted into (2.5) to finally obtain an emittance.

3.3 Automated procedure

As mentioned, the motors and cameras on the emittance meter can be controlled remotely by TANGO, and in effect MATLAB as well. To facilitate the binding between the two, a framework has been built in-house for MATLAB. It consists of a class for a generic device that defines certain attributes. The generic class for an attribute supports reading and writing values. For the automation procedure, two subclasses of the device class are created for a motor and a camera. The motor defines an attribute for its position, and two methods for reading and writing to it. The camera defines an attribute for its image sensor and a method for reading its pixel values. The motor class were then tested by linking it to an actual motor and it worked as expected. A procedure for the measurement could then consist of creating four motor objects linked to the four different motors on the emittance meter as well as a camera object. Then a range of data points is defined and iterated through. On each iteration, the slit is moved to its longitudinal position and then scanned through the beam, if a single slit is used, while the images are saved by the camera class. When the loop is done, the procedure calls the emittance estimation script, which iterates through the images and estimates the emittance for each longitudinal position.

3.4 Gun conditioning and emittance measurement

When the electron gun was put in place and roughly aligned, it was then connected to RF power via a wave guide and sealed with the valve positioned after the solenoid. The solenoid was placed as close to the cathode as possible and ion pumps were connected to each side of the gun. The system was then pumped to a pressure of 4×10^{-9} mbar and checked for leaks before the valve was opened up to the intermediate part connecting it to the emittance meter. Lastly, the valve to the emittance meter was opened and the whole system was confirmed to be sealed.

The gun was then conditioned, a procedure where the breakdown voltage of the gun is gradually increased. An unconditioned gun has a very low breakdown voltage, meaning it will spark at voltages well below the intended voltage of the gun, since the metal surface is to a certain degree covered by adsorbed gas layers [19]. Impurities and protrusions in the surface of the metal create sharp spikes in the electric field, causing discharges between anode and cathode. Depending on the discharge energy, the sparking can either smooth the surface by removing the contaminants or create new protrusions. A low energy discharge, which smooths the surface,

therefore increases the breakdown voltage of the cavity, while an energetic spark can render the gun useless. To avoid this, the RF power was gently increased in small steps, allowing small discharges at each step. The discharges were seen on the oscilloscope, which displayed the field inside gun, but also on the pressure levels, which abruptly rose as the impurities were removed from the surface. The set field in the klystron reached a level of 24 kV before the conditioning had to be postponed.

Due to a time constraint and unforeseen obstacles along the way, the measurements are unfortunately left out of this thesis. The gun behaved nicely during conditioning, but the dark current[1] could not be detected even at 24 kV, where it had been detected in earlier conditioning. This points to a misalignment of the gun, which can take weeks to correct for. Another possibility is that the klystrons supplied a much lower power at the same level of voltage than before. A measurement of the power suggests that the klystron supplied 2.7 MW of power at 23 kV as opposed to 4.55 MW during earlier conditioning. Continued conditioning could have corroborated this notion, but since the laboratory were scheduled to be occupied by other projects at this time, all measurements had to be postponed. Older images taken from when the emittance meter was originally put in place in 2008 will be analyzed instead. These images were taken using a single slit method, as opposed to a multi-slit described in section 2.3, meaning the single slit is panned across the width of the beam between shots.

More recently, the electron gun was used to take a series of pepperpot images. One of these images is seen in figure 3.6 where the colors have been inverted and the contrast increased for greater visibility. The image is part of a series of emittance measurements taken for different phases of the electric field in the electron gun. For each phase data point there were a dozen images captured to allow for averaging of the data. These images were fed to the same script that estimated the emittance during the simulations. The procedure of calculating the emittance was naturally very similar to the simulated one. However, the pictures contained some artifacts in the lower right corner which had to be excluded to get an accurate reading. They contained a lot of noise as well, but the peaks were still discernible for the script. Regardless, the data was smoothed with a gaussian filter to remove the possibility of the script mistaking the noise for a peak.

[1] Dark current is the emission of electrons from cold metals in intense electric fields [20]. The work function of the metal is reduced by the field which increases the probablity of an electron tunneling through the surface barrier.

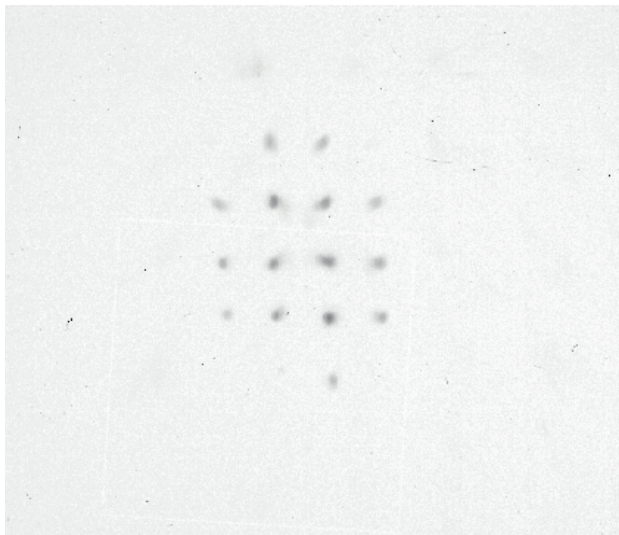

Figure 3.6: Pepperpot image - Image of the electron distribution at the phosphor screen. The contrast has been increased and the colors inverted to enhance the visibility of the spots.

4

Results

In this chapter I will present results from 4 different systems, which for the purpose of this thesis can be considered the same. The first one is the system developed during this thesis work. The second one is a system developed by an Italian group. They used the same emittance meter, attached to a slightly different setup. Then there is the pepperpot measurement that a group at MAX IV built, which used a similar gun but a different solenoid. Lastly, there is the simulated setup, which is a close copy of the developed setup.

4.1 Simulations

4.1.1 Emittance evolution

The shape of the laser pulse was set to be either gaussian or a flat top, with a certain σ in the first case and a rise time and FWHM in the latter. The difference in the emittance between these two pulse shapes is seen in figure 4.1 where FWHM $= \sigma = 6$ ps and the rise time 0.5 ps. The emittance is plotted in blue and the beam envelope in red. The gaussian pulse gives rise to the larger emittance, while they both show the same beam envelope evolution. Clearly, the plateau shape is achieving a smaller emittance. Consequently, the parameters of the plateau was then varied. In figure 4.2 the FWHM was gradually increased, and the emittance evolution responded by moving the slowly disappearing local maximum closer to the cathode. The beam envelope behaved similarly. On the other hand, when the rise time was increased instead, the beam envelope was practically unchanged, as seen in figure 4.3. The local maximum of the emittance seems to disappear as the rise time increases. With the FWHM set to 6 ps and the rise time to 0.5 ps, the total charge of the bunch was examined. In figure 4.4 the charge

was increased from 0.1 nC to 0.5 nC which led to rapid increase of the emittance. It is not surprising that a lower charge gives a lower emittance. With the charge set to 0.1 nC the effect of the horizontal size on the emittance was evaluated as seen in figure 4.5. The bunch size has a dramatic impact on the emittance, it not only removes the double minimum behavior but increases the emittance very rapidly afterwards. A transverse rms size of 0.7 mm was chosen for the remaining simulations, which is comparable to an actual laser beam profile.

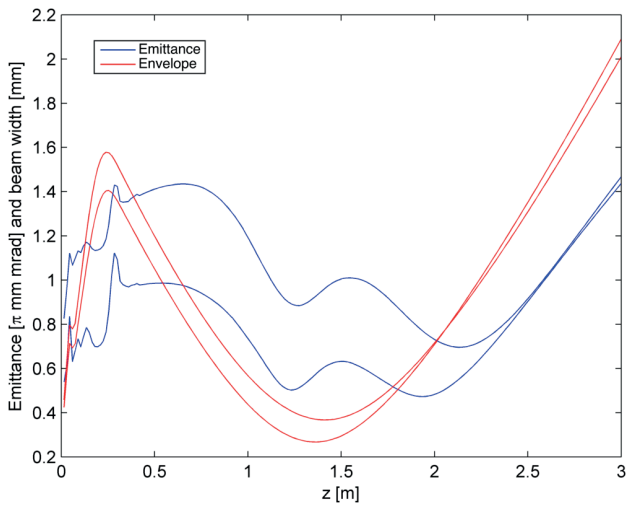

Figure 4.1: Gaussian vs Plateau pulse shape - A comparison of a gaussian and a plateau pulse shape for $FWHM = \sigma$. The curve with the larger emittance is attributed to the gaussian pulse shape.

Figure 4.6 shows a solenoid scan, where a maximum electric field of 86 MV m^{-1} was used with a phase of 47°. The maximum magnetic field was scanned from 0.1285 T to 0.1985 T and the double minimum behavior, highlighted in the figure, was found with a maximum strength of 0.1685 T. In figure 4.7 the same lines are highlighted in a much narrower scanning interval, from 0.1605 T to 0.1705 T. The double minimum behavior is present for all variations, but only for 0.1685 T is the local maximum located at roughly 1.5 m. This is not emittance compensation however, since the beam focus does not line up with the local maximum of the emittance. By slightly changing the other parameters proposed here, it should be possible to move them closer to each other so that they eventually line up in the vicinity of $z = 1.5$ m.

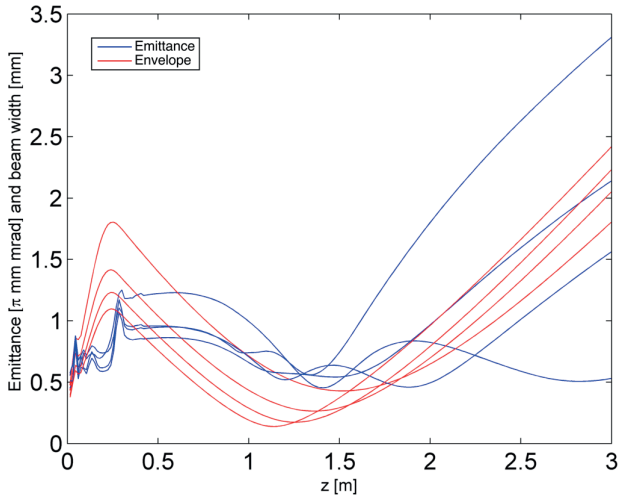

Figure 4.2: Plateau pulse shape - The plot shows the emittance evolution when the FWHM of the plateau shaped laser pulse was increased.

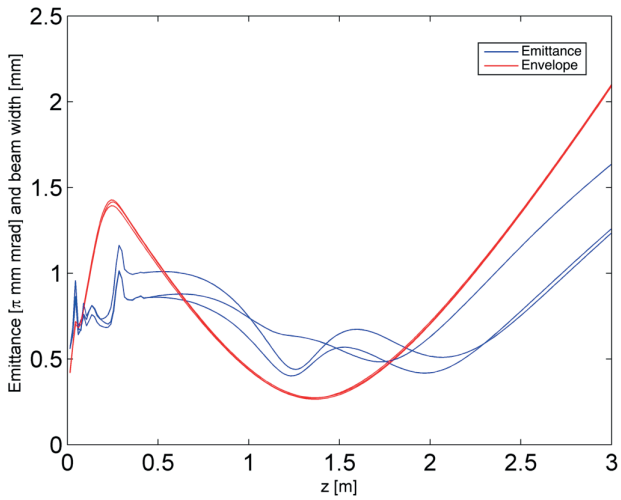

Figure 4.3: Plateau pulse shape - The plot shows the emittance evolution when the rise time of the plateau shaped laser pulse was increased.

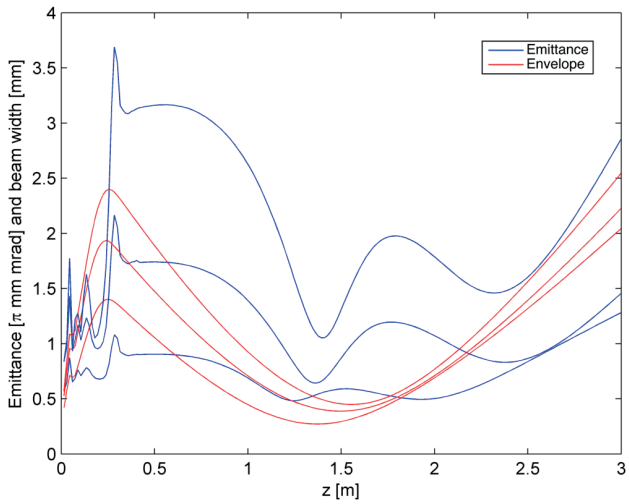

Figure 4.4: Total charge - The plot shows the emittance evolution when the total charge of the bunch was increased.

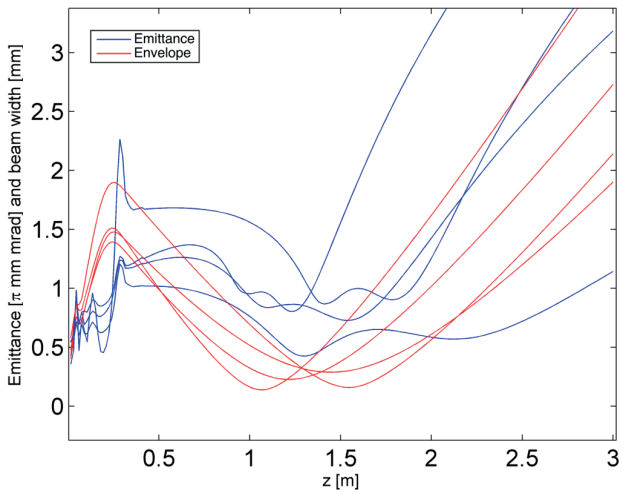

Figure 4.5: Horizontal size - The plot shows the emittance evolution when the horizontal size of the bunch was increased.

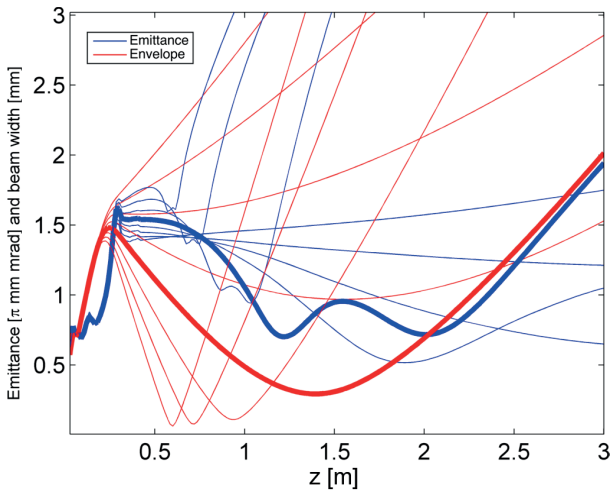

Figure 4.6: Solenoid scan - The emittance and beam envelope for a solenoid scan from 0.1285 T to 0.1985 T.

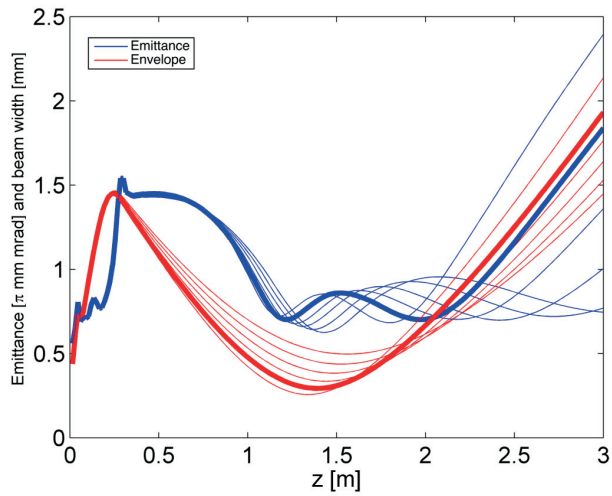

Figure 4.7: Solenoid scan - The emittance and beam envelope for a solenoid scan from 0.1605 T to 0.1705 T.

4.1.2 Pepperpot simulation

The pepperpot script was run for a wide variety of parameters, not only varying the field strengths and phase, but also the pepperpot position, the screen position and the pepperpot dimensions. A typical electron distribution, generated and tracked by Astra, is seen in figure 4.8 just before it enters the (hypothetical) pepperpot at $z = 1.5\,\mathrm{m}$. The solenoid field was set to 0.1575 T. As seen the distribution is roughly 6 mm wide and tall which means a hole spacing of 1 mm is reasonable. The same particle cloud after it has been stripped by the pepperpot is seen in figure 4.9, and in figure 4.10 the cross section is taken at the location of the screen.

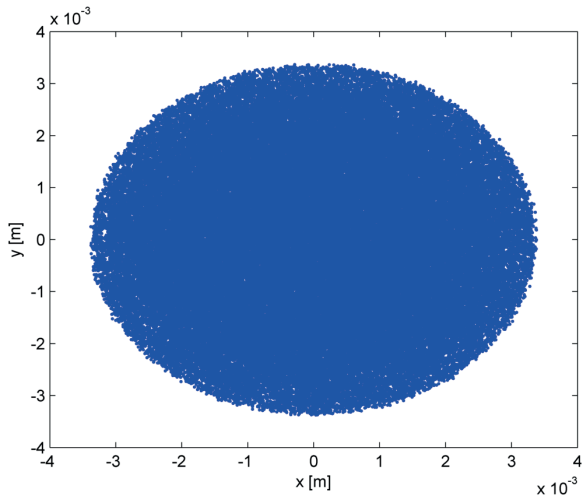

Figure 4.8: Electron distribution 1 - A cross section of an electron distribution from Astra just before it enters the pepperpot.

Another distribution is shown in figure 4.11, generated with a stronger solenoid field of 0.1805 T. The beam envelope is much smaller than before, requiring a pepperpot with narrower spacing and smaller holes. The remaining particles in figure 4.12 were obtained using a spacing of 300 µm and a hole radius of 30 µm. With a distance of 0.3 m to the screen the resulting spot sizes at the screen are shown in figure 4.13. When an image like the one in figure 4.13 is summed over horizontally and vertically, one obtains a graph like the one in figure 4.14. The script has tried to fit a gaussian curve to each peak and shows the residual below. The information about the peaks that is visible in the figure is used to calculate the emittance.

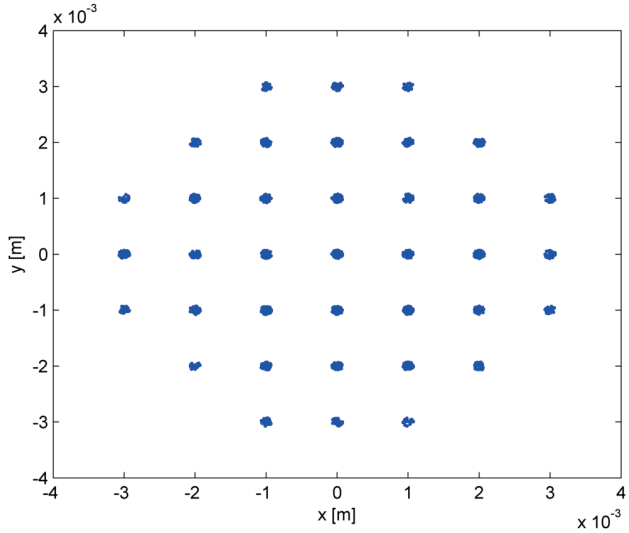

Figure 4.9: Electron distribution 1 - A cross section of an electron distribution from Astra just after the pepperpot.

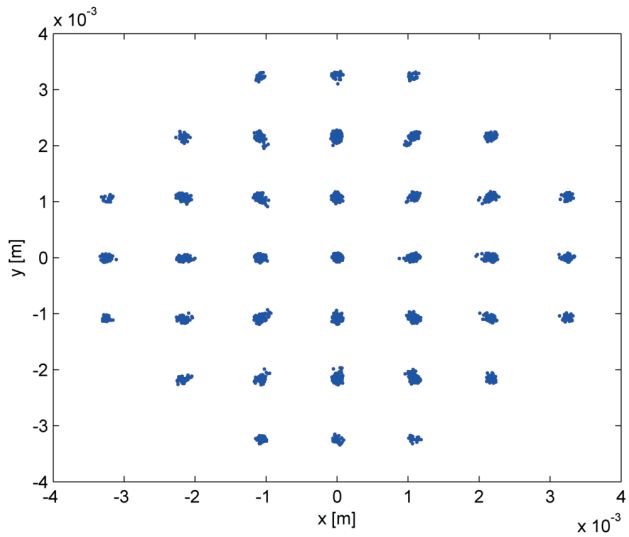

Figure 4.10: Electron distribution 1 - A cross section of an electron distribution from Astra at the screen.

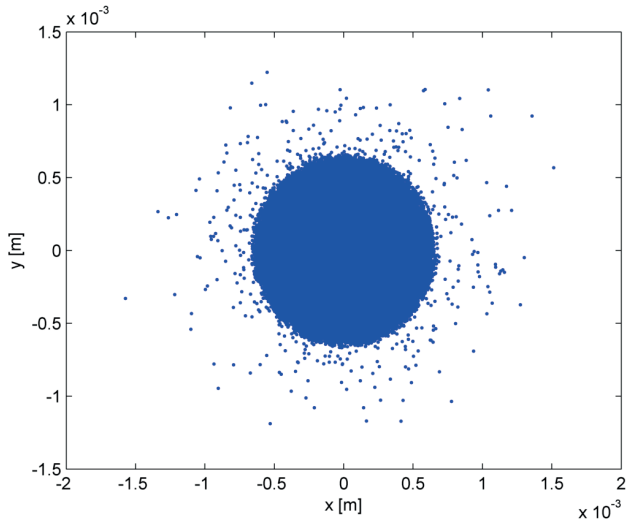

Figure 4.11: Electron distribution 2 - A cross section of an electron distribution from Astra, with a smaller beam envelope.

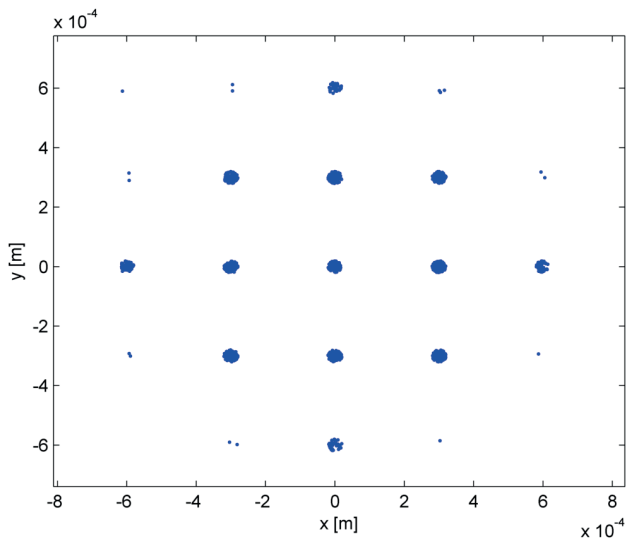

Figure 4.12: Electron distribution 2 - A cross section of an electron distribution from Astra just after the pepperpot

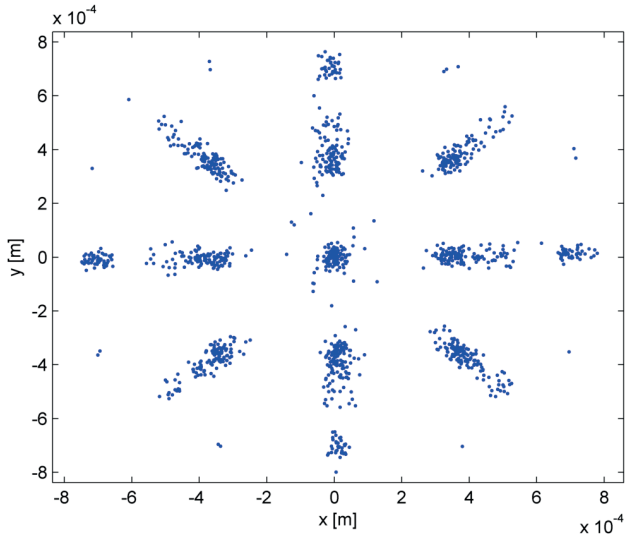

Figure 4.13: Electron distribution 2 - A cross section of an electron distribution from Astra at the screen.

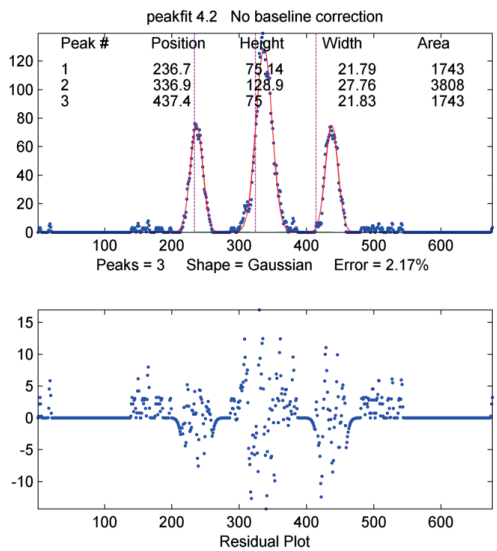

Figure 4.14: Detection and fitting - Plot of the visual output from the peak detection and fitting script.

The script was then run for six different positions of the pepperpot, ranging from 1.3 m to 1.8 m in equal intervals, with the parameters seen in table 4.1. This was done in order to see if the estimated emittance follows the same evolution pattern as the real one. The result is seen in table 4.2 where both horizontal, normalized trace space emittance from Astra (the "real" emittance) and the estimated one are tabulated. These values are then plotted in figure 4.15 as a function of pepperpot position. The red graph is the real emittance and the blue graph is the estimated. It seems that the script, at least for these settings, is constantly underestimating the emittance while maintaining the same overall shape as the real emittance. Another simulation, with the magnetic field set at 0.1755 T instead, corroborates this notion as seen in figure 4.16. The two simulations used the same pepperpot dimensions, but since the latter had a wider beam envelope, five spots in both directions showed up, instead of three. Clearly the script performs comparatively in either case. The underestimation is distressing, and beyond 1.7 m the first simulation started to behave weirdly when the beam envelope increased rapidly, causing the emittance to be overestimated instead. This could be a result of the relatively low particle count. Another source of error could be that multiple spots that wind up in the same area in the MATLAB plot only counts as one spot, that is the plot is basically black and white, potentially neglecting a large amount of particles. This is not a problem with the images taken with the experimental setup.

E_{max}	$90\,\mathrm{MV\,m^{-1}}$
B_{max}	0.1805 T
ϕ	37°
Hole radius	50 µm
Hole spacing	500 µm

Table 4.1: Parameters used in the pepperpot script.

Position [m]	"Real" emittance [π mm mrad]	Estimated emittance [π mm mrad]
1.3	0.468770	0.118402
1.4	0.539750	0.192585
1.5	0.569850	0.213911
1.6	0.576970	0.233924
1.7	0.535110	0.198746

Table 4.2: The real horizontal, normalized trace space emittance and the estimated one.

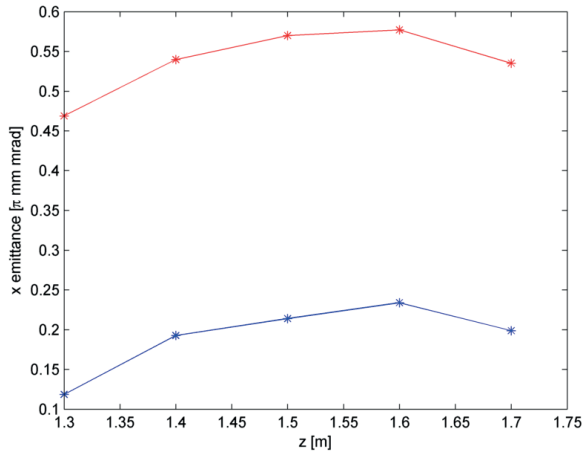

Figure 4.15: Emittance comparison - Plot of the horizontal, normalized trace space emittance as a function of longitudinal position. The real emittance from Astra is shown in red and the estimated ("measured") is shown in blue.

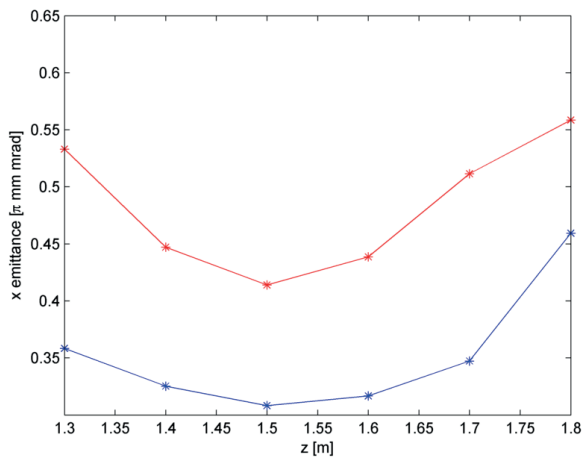

Figure 4.16: Emittance comparison 2 - Plot of the horizontal, normalized trace space emittance as a function of longitudinal position. The real emittance from Astra is shown in red and the estimated ("measured") is shown in blue.

4.2 Experimental data

The same script that estimated the emittance in the simulations was fed the images taken previously with the pepperpot setup. The output from the script is seen in figure 4.17 where an image has been summed over horizontally. The entire signal is shown in the lower domain while the upper contains a zoomed-in part of the signal, showing the curve fitting. As mentioned earlier, the signal is noisy but the script still detects the peaks. The artifact to the right of the peaks stems from that the images are not completely dark below the spots, and these pixels add up to a very strong signal. To remove or suppress the artifact, a handful of images had been taken without the beam spots, which were then averaged and subtracted from the signal. A reduced signal is shown in figure 4.18, where the artifact is attenuated and the noise level is lower. When subtracting the background, some very sharp spikes emerged. These could sometimes be mistaken for a peak which led to a false emittance reading. The smoothing of the signal removed nearly all noise, as seen in figure 4.19.

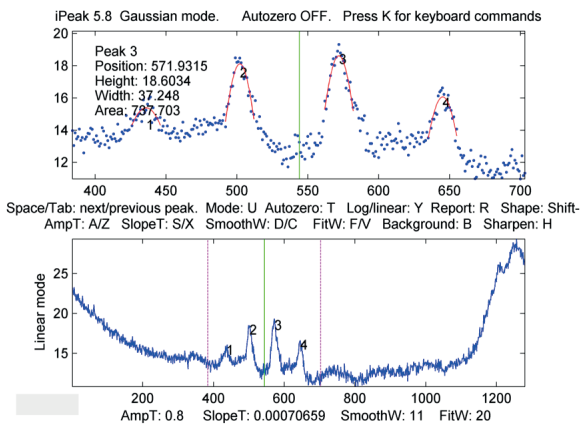

Figure 4.17: Detection and fitting 2 - Plot of the visual output from the peak detection and fitting script used on the measured images. The image was summed horizontally.

The images taken for different phases of the electric field in the electron gun were then analyzed with a MATLAB script, estimating the emittance of each one. The resulting plot in figure 4.20 shows the estimated emittance against the phase of the electric field, for three different measurements A, B and C. The standard deviation for the data points is not negligible, partly stemming from the fact that the peak finding script is not fully reliable. It might miss

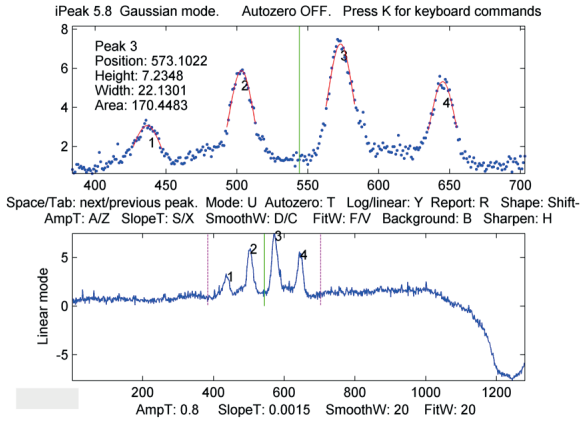

Figure 4.18: Detection and fitting 3 - Plot of the visual output from the peak detection and fitting script with the background noise subtracted. The image was summed horizontally.

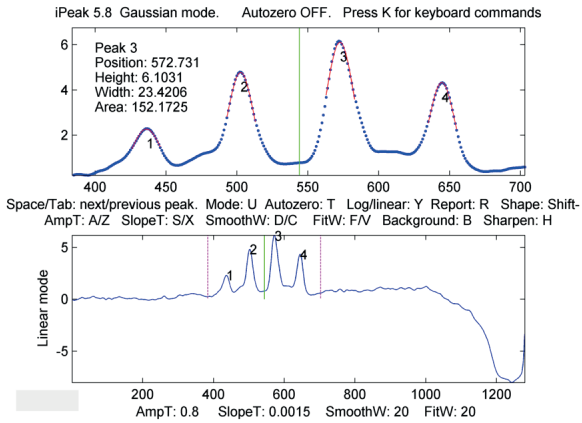

Figure 4.19: Detection and fitting 4 - Plot of the visual output from the peak detection and fitting script with the background noise subtracted and the signal smoothed. The image was summed horizontally.

a peak or two if the signal is not a good match for the peak detection settings. The script's influence on the standard deviation was however greatly diminished with the noise reduced signal. Measurement A and B were taken with a charge of 0.1 nC and C with 0.3 nC. As seen A and B are quite close in estimated values and show the same evolution curve, as is expected. Measurement B shows a greater error for some points due to a varying quality of the signal.

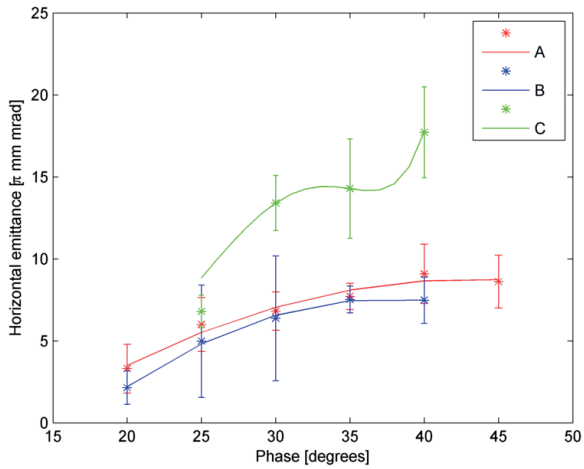

Figure 4.20: Estimated emittance - The estimated emittance as a function of phase, calculated from roughly a total of 200 images taken for three measurements.

The script was then modified to be able to estimate the emittance from the single slit experiment as well. The images were individually summed over and the single peaks were detected in each of them. In figure 4.21 the peaks are shown alongside the source images, which have been overlaid into one figure. The measurement, which was done by the Italian group from Trieste, only captured images of the beamlets at a fixed position from the cathode. The pictures that they have shared used an electron beam energy of 5.2 MeV which corresponds to a relativistic gamma factor of 11.18. The vertical normalized emittance was then estimated from a total of 15 measurements to a value of $2.4(2)\,\pi$ mm mrad. The number can then be compared to that of the Italian group, which was in the range of $2.2(2)\,\pi$ mm mrad.

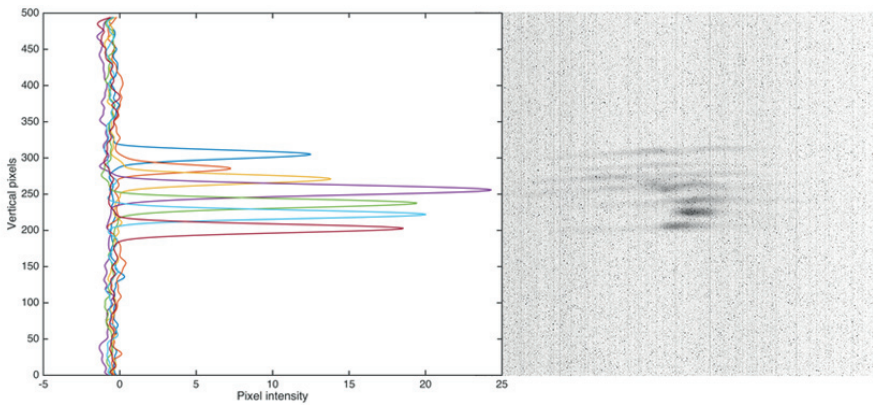

Figure 4.21: Single slit measurement - The seven single slit images have been overlaid into one image on the right, where the colors have been inverted. On the left the seven peaks are shown as well

5

Conclusion

This thesis is about the development and implementation of a system for measurement of the emittance. As mentioned the setup could not be tested in time for this thesis. The project will however continue after this thesis work is done and in the beginning of 2015 it can be expected to produce results.

The system is working as intended. The preliminary aims, of simulating the electrons and developing a script for estimating the emittance, were also met. The script for automating the measurements could not be fully tested, but the individual parts that were developed did work.

The simulations in Astra provided insights on how the different parameters affected the emittance and beam envelope. The shape and size of the laser pulse as well as its energy greatly affected the outcome. The simulations also imply that it is possible to find the working point in the vicinity of the linac entrance, although there exists a better fit than the one found here. Preferably, the envelope focus and the local maximum of the emittance should line up with each other.

Using MATLAB together with Astra a model was developed which reflects an actual emittance measurement. The simulation performed rather well, but had one or two issues. If a heat map combined with a higher particle count had been used, the images would be expected to resemble the real ones much more than the likes of figure 4.10. The heat map would ensure that multiple electrons in the same pixel spot would be counted more than once, which could result in a more precise emittance estimation. The computational time of this simulation was a major bottleneck in the development of the script. Using 100 000 particles a single simulation was timed at 30 min. Both MATLAB and Astra should support multi-core operations, but it was

far from trivial to implement them. If this could have been done, it would have dramatically cut the computational time.

This thesis was concluded with an analysis of earlier measurements, indicating that the implemented emittance estimation method works. The single slit images provided a very consistent signal resulting in a relative standard deviation of 6 %, which can be compared to the huge error bars in figure 4.20 where the single shot pepperpot technique was used. The difference between the two is that the single slit generates a much stronger signal, while completely avoiding the risk of having beamlets overlap on the screen. A disadvantage is of course the increased time of measurement.

There are a few things left to be done before the setup can be used seamlessly. The electron gun needs to be further conditioned in order to be able to detect some dark current, especially if the klystron is actually down on power. When the dark current is detected, it can be used to align the gun. This will be challenging since the first screen is more than a meter away from the cathode. To speed up the alignment process a second screen could be added closer to the cathode, in front of the laser chamber where the aperture is the smallest. A bigger problem is that the screen is 1.7 m from the cathode. Between the laser chamber and the cathode there is not a lot of flexibility for reducing the distances.

Then, the emittance meter can finally be used to obtain a plot of the emittance evolution. Depending on if the local maxmimum appears or not, the fields may need to be tweaked a bit until the maximum appears at about 1.5 m. If this behavior is found, emittance compensation could be implemented and the existing linac structure at MAX IV would deliver a beam suitable for an FEL.

References

[1] Primoz Rebernik Ribic and G. Margaritondo. **Status and Prospects of X-ray Free-electron Lasers (X-FELs): A Simple Presentation**. *Journal of Physics D: Applied Physics 45.21*, 2012. 11

[2] Klaus Wille. *The Physics of Particle Accelerators, an introduction*. Oxford University Press, New York, 2005. 11, 14

[3] Peter Schmüser, Martin Dohlus, and Jörg Rossbach. *Ultraviolet and soft x-ray Free electron lasers*. Springer, Berlin, 2008. 12

[4] **Visions**. URL: `https://www.maxlab.lu.se/node/1055` [cited 2014-08-05]. 10

[5] **MAX IV FEL** [online]. URL: `https://www.fels-of-europe.eu/facilities/x_ray_facilities/max_iv_fel/` [cited 2014-12-02]. 10

[6] J. Buon. **Beam phase space and emittance**. Technical report, Laboratoire de L'Accélérateur Linéaire, Orsay, 1992. 13

[7] Barletta, Spentzouris, and Harms. **USPAS notes on emittance**. URL: `http://uspas.fnal.gov/materials/10MIT/Emittance.pdf` [cited 2014-08-25]. 14

[8] G. Dattoli et al. **Slice emittance, projected emittance and properties of the FEL SASE radiation**. Technical report, 2010. 15, 16

[9] M. Ferrario et al. **HOMDYN Study for the LCLS RF Photo-Injector**. Technical report, SLAC, 2000. 15, 16

[10] Min Zhang. **Emittance formula for slits and pepper-pot measurements**. Technical report, Fermi National Accelerator Laboratory, 1988. 17, 18, 19

[11] Klaus Flöttmann. **Pepper pot design for space charge dominated high brightness beams**. Technical report, DESY, 1996. 20

[12] M.A. Zucker M.J. Berger, J.S. Coursey and J. Chang. **Stopping-Power and Range Tables for Electrons, Protons, and Helium Ions**. URL: `http://www.nist.gov/pml/data/star/index.cfm` [cited 2014-09-30]. 20

[13] L. Catani et al. **Operational Experience with the Emittance-Meter at SPARC**. Technical report, 2006. 21, 22

[14] **TANGO**. URL: http://www.tango-controls.org/ [cited 2014-10-30]. 21

[15] **MAX IV RF gun** [online]. URL: https://www.maxlab.lu.se/node/1722. 22

[16] **MAX IV RF gun** [online]. URL: https://www.maxlab.lu.se/node/859 [cited 2014-12-02]. 22

[17] **ASTRA** [online]. URL: http://www.desy.de/~mpyflo/Astra_dokumentation/Astra-Manual_V3.1.pdf [cited 2014-12-02]. 24

[18] Tom O'Haver. **Peak Finding and Measurement**. URL: http://terpconnect.umd.edu/~toh/spectrum/PeakFindingandMeasurement.htm#findpeaksfit [cited 2014-09-03]. 26

[19] D. Köning J. Ballat and U. Reininghaus. **Spark conditioning procedures for vacuum interrupters in circuit breakers**. *IEEE Transactions on Electrical Insulation*, 28(4), August 1993. 27

[20] R.H. Fowler and L. Nordheim. **Electron Emission in Intense Electric Fields**. *Proceedings of the Royal Society of London. Series A, Containing Papers of a Mathematical and Physical Character*, 119(781), 1928. 28

Declaration

I herewith declare that I have produced this paper without the prohibited assistance of third parties and without making use of aids other than those specified; notions taken over directly or indirectly from other sources have been identified as such. This paper has not previously been presented in identical or similar form to any other Swedish or foreign examination board.

The thesis work was conducted from Marcus Isinger under the supervision of Dr. Francesca Curbis and Joel Andersson at MAX IV laboratory.

Lund

LUND
UNIVERSITY

Series of Master's theses
Department of Electrical and Information Technology
LU/LTH-EIT 2015-424

http://www.eit.lth.se